The optical efficiency of three different geometries of a small scale cavity receiver for concentrated solar applications

Daabo, Ahmed; Mahmoud, Saad; Al-Dadah, Raya

DOI:
10.1016/j.apenergy.2016.07.064

Document Version
Peer reviewed version

Citation for published version (Harvard):
Daabo, A, Mahmoud, S & Al-Dadah, R 2016, 'The optical efficiency of three different geometries of a small scale cavity receiver for concentrated solar applications', *Applied Energy*, vol. 179, pp. 1081–1096. https://doi.org/10.1016/j.apenergy.2016.07.064

The optical efficiency of three different geometries of a small scale cavity receiver for concentrated solar applications

Ahmed M. Daabo[a,b*], Saad Mahmoud[a], Raya K. Al-Dadah[a]
[a] The University of Birmingham, School of Engineering,
Edgbaston, Birmingham, B15-2TT, UK
[*]Email: axd434@bham.ac.uk
[b] The University of Mosul, Mech. Eng. Dept. Iraq

Abstract

The demand for energy is continually increasing day after day; but at the same time, investigations around the world into sustainable sources of power are growing in number. Concentrated Solar Power (CSP) can act as an efficient low cost energy conversion system to produce electricity which could lead to reducing the continuous demand on conventional fossil fuels. Most of the literature concerning CSP concentrates on the heat losses and their relationship to the receivers' geometries; where these receivers are evaluated according to their thermal efficiency. The majority of the literature has often neglected heat gain enhancement by the receivers' geometries, which helps to increase the heat transfer to the working fluid. This work concentrates on the optical efficiency as well as the heat flux distribution of three different geometries. The cylindrical, conical and spherical geometries of a cavity receiver are considered with the objective of analysing their optical and thermal behaviour optically and thermally, using the ray tracing method and a Computational Fluid Dynamic (CFD) model. The results showed that the conical shape of the receiver gathered, as well as absorbed, a higher amount of reflected flux energy than the other shapes, with about 91% and 82% for 75% and 85% absorption ratios respectively. The cavity receiver shapes and their absorption ratio are key parameters which affect the focal point location; thereby there is an optimum distance for each design depending on these two parameters. The results of the simulated work are validated using the experimental work found in the literature. Overall, in order to evaluate the heat balance, 3-D thermal analysis was employed using Fluent 15 and the amount of heat losses for the three shapes was determined. It was observed that the conical shape receiver experienced a lower heat loss. To ensure more confidence in the results, the thermal outcomes were validated against experimental works in the literature and they demonstrated good agreement.

Keywords: Concentrated solar plant, Ray-tracing, Optical efficiency, Solar receiver, Thermal analysis.

1- Introduction

Solar radiation is collected by different types of Concentrating Solar Collectors (CSC) and focused into thermal receivers in order to be converted to the thermal energy of Concentrated Solar Power (CSP). With the existing energy demand and environmental dilemmas the technology of solar energy has an essential role [1]. The Heat Transfer Fluid (HTF) is pumped to the thermal receiver to carry the thermal energy in order to drive one of the power cycles such as the Rankine cycle, the Organic Rankine cycle, the Stirling cycle and the Brayton cycle [2]. The CSP with the Brayton Cycle (BC) has the potential to offer higher efficiency, lower cost and pressure losses compared to other cycles [3, 4].

Thermal analysis of different types of receiver was investigated: central [5-8], trough [9- 13] and volumetric types [14-17]. Furthermore, for the cavity receiver types' heat losses analysis and their

connection with receiver geometries, dimensions and positions were investigated for different applications [18- 25]. Amongst the literature [18- 25], the most relevant have been chosen and will be discussed in the next paragraph.

Harris and Lenz [18] assessed the thermal performance of five different geometries of cavity receivers (cylindrical, heteroconical, spherical, elliptical and conical) with a parabolic concentrator. Their results showed that the losses of the cavity receiver are about 12% of the input energy to the aperture of the receiver and there is a small effect from the cavity geometry on the overall efficiency. Reddy et al. [21] studied the effect of different factors such as the emissivity, inclination, insulation thickness and operating temperature on natural and forced convection and radiation heat losses of a modified hemispherical cavity receiver. Regarding the effect of the receiver inclination, they found that the minimum natural convection heat loss occurs when the open side of the receiver faces downwards, i.e. at 90^{o}. Also, a correlation for the Nusselt number for radiation and the convection heat transfer losses' calculation has been proposed. Roux et al. [22] analyzed theoretically a modified cavity receiver combined with a parabolic dish concentrator used in a small scale CSP-BC system. Many design parameters were studied, including the tube diameter, tube length of the thermal receiver, rim angle, inclination receiver, concentration ratio and mass flow rate. The results showed that the channel length is affected by the wind factor, rim angle and concentration ratio and that the thermal receiver design has a significant effect on the net power output of the system. Prakash [23] studied the natural convection heat losses of different diameters of a cylindrical cavity receiver based on CFD simulations. The model included flow inside a helical coil with air as an HTF. The results showed that the increase in the convection losses is due to the increase in the mean temperature of the HTF and to the opening ratio as well; while a decrease in the convection loss is due to the increase in the receiver inclination.

However, there is still some ongoing research regarding the optical characterisation for other kinds of receivers in the literature. For example, a single and double elliptical pipe receiver was studied by Abdullahi et al. [26]. They analysed a Compound Parabolic Concentrator (CPC) with this type of receiver in different configurations. The results showed that the optical efficiency of a horizontal and vertical double receiver is greater than the single receiver by 15% and 17%, respectively. Roux et al. [27] evaluated optically a tubular receiver in terms of different variables such as; concentrator shape, reflectivity, diameter, rim angle. They also studied different receiver factors such as; aperture area, material and tube diameter, working fluid mass flow rate, inlet temperature through the receiver with the aim of finding the receiver's surface temperature and its efficiency. The results revealed that the optimum area ratio depends directly on both optical and tracking errors. They concluded that the receiver efficiency can be raised up by increasing the dish reflectivity and also by increasing the precision of both the optics and dish surface. Furthermore, enlarging the receiver tube and decreasing the mass flow rate decreases the efficiency of the collector because of the high receiver surface temperature. Qiu et al. [28] numerically and experimentally investigated the performance of a cylindrical cavity receiver with its helical tube using five lamps of Xe-arc light source with splitter placed at the bottom of the receiver to distribute the received flux. Their experimental results showed that with a 300 kW/m^2 average flux and 5 m^3/h of air volume flow rate, the air outlet temperature can reach up to 800oC. Also, deviation between theoretical and the experimental results ranged between 2.5 % to 8%. A model of multi-cavity receiver for high concentrated flux was analysed by Fleming et al. [29]. The study was carried out on a simple model designed with all the necessary parameters for analysing its thermal efficiency by applying an optimal value and distribution of flux. Based on their results, they concluded that there is high potential of achieving more than 90% thermal efficiency from the receiver at absorptivity greater than 99.8% and heat transfer coefficient of the working fluid ranging 250 to 500 $W/m^2/K$. Algarue et al. [30] investigated the effects of concentration ratio on three

types of reflective concentrator solar collectors as well as two types of refractive concentrator solar collectors using OptisWorks®. Their results showed that optical efficiency for all collectors is about 80% when the concentration ratios up to 10X, while the optical efficiency for reflective and refractive concentrators is 30% and 80 %, respectively at concentration ratio 20X. Wang et al. [31], tried to increase the optical efficiency of cylindrical cavity receiver by exploiting the dead space, the area which cannot be coiled by the absorber tube, by using two different techniques. The first one was combining the cylindrical receiver with a conical shape at the dead area and the second was by changing the height of the interior convex surface. The results showed that some improvement on the optical efficiency can be done during changing the dimensions of the interior vortex shape which can covered the dead area of the studied receiver. Enhancing the thermal performance of solar receiver through the focusing on the optical characteristics was tried by Weinstein et al. [32]. In their research they tried to decrease the thermal losses, especially the radiative one, by applying the directional selectivity idea which leads to a reduction in the mentioned heat loss by 75% and as a result reaching high receiver efficiency for solar thermal applications. Tzivanidis et al. [33] evaluated the thermal and optical efficiencies for a parabolic trough collector. In their study, they investigated the optical and thermal performance, in terms of absorbed flux and temperature distribution, of a small scale parabolic trough at different boundary conditions. Their results showed that the model that had been used was efficient.

2- Cycle components

The CSP-Brayton cycle, shown schematically in Fig. 1, consists of a compressor (1-2), thermal receiver (3-4) and a turbine (4-5). The thermal receiver is considered the heart of the system because it provides the cycle with the required thermal energy; thus increasing its efficiency by reducing the optical and thermal losses, which will increase the overall system's efficiency. A recuperator, (2- 3), is used to recover heat from the turbine exit's hot air.

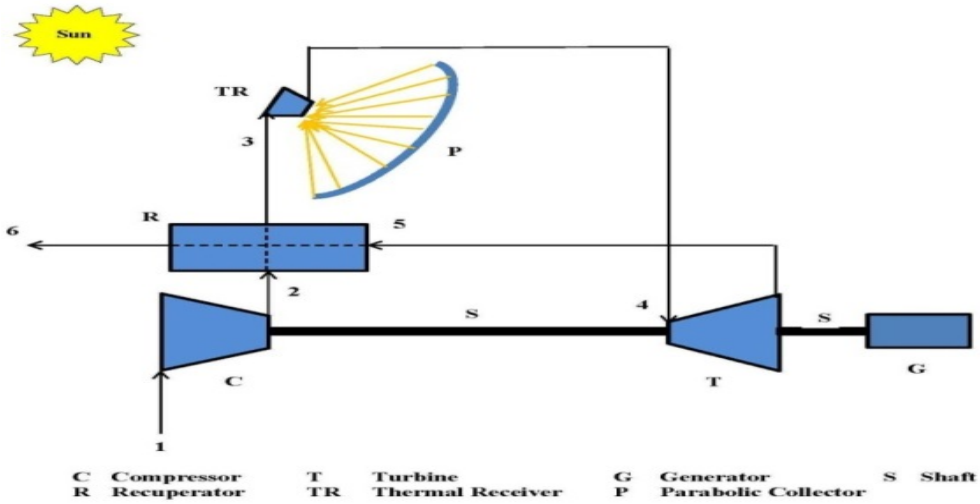

Fig. 1. Schematic diagram of CSP-BC system.

3- Methodology

The geometry of each cavity receiver is drawn using SOLIDWORKS® 2015, by considering the surface and aperture areas' equality as shown in Table (1). The energy was represented by the

amount of rays which the OptisWorks® 2012 software provides; more detail about this software is discussed in section 6. Monte- Carlo algorithm was used for analysis in OptisWorks® 2012 as it is a well-known methodology for robust simulation. This method assumes that a large number of rays are going to take their own random paths when they hit the surfaces. Each of the single rays transmits the same amount of energy and has a certain direction which is already determined from the appropriate probability density function. Depending on the surface properties, emissivity, reflection and absorption, each of these rays will take a specific path which is specified by a set of statistical relationships.

The 2-D detector can read only equal reflected power that passes through the aperture area of each receiver shape. However the 3-D detector is able to read exactly the values of flux at every single plane and by doing that the effect of the geometry has been highlighted as a main factor, in terms of both the amount of received flux and the distribution. Different impinging arrangements including the receiver's shape, the receiver's focal plane position as well as the receiver's wall absorption ratio, are examined based on the ratio of received flux and the absorbed flux with respect to the energy loss. Finally, the thermal balance for the three shapes was evaluated in terms of the amount of heat loss and the absorbed heat by the working fluid. In this study the chosen reflector is 1 m diameter and 45^{o} rim angle, as it gives maximum concentration ratio, Fig. 2 [34].

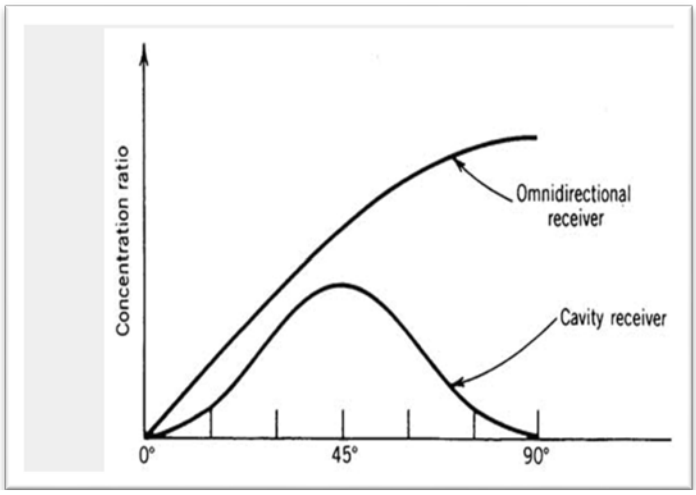

Fig. 2. The relation between the geometrical concentration ratio and rim angle.

4- Optical losses

Optical losses are mainly associated with either manufacturing and construction imperfection or material properties. Based on the literature found in [35-39], these types of losses can be summarised as follow:

- Spillage losses are part of radiation hitting outside the aperture of receiver which can add about 1–3% to the loss.

- Shading losses are related to the ratio of the reflective area of the dish which is shadowed by the receiver. However, this type of loss can be minimized if the dish aperture area is considerably larger than the receiver.

- Reflective losses are the difference between reflected energy and energy falling on the reflective or receiver surface areas. Depending on the material properties, this loss can represent about 6 to10% from the incoming or received energy.

- Transmission losses can be defined as the amount of energy which is lost in the air when it moves from the reflector to the receiver which can add about 2 to 4 % to the loss.
- Absorption losses are the incoming or received energy that can be absorbed by the reflector or the receiver material, which causes thermal stresses.

- Cosine losses can be defined as the difference between total reflective area and its projected area, as it is seen from the sun.

At this point it is worth to mention that first five types of the mentioned losses are automatically included in the analysis of this study. Obviously, the optical efficiency is influenced by the combination of the mentioned losses above. Moreover, the accompaniment errors like those of structure, tracking, alignment and sensor should also be considered in experimental studies. The optical efficiency of the reflector can be expressed using equation (1), whereas the optical efficiency of the receiver can be determined using equation (2),

$$\eta_{oRef} = \frac{Q_r}{Q_s} \quad (1)$$

Where Q_r, is the energy reached to the receiver and Q_s is the incident falls on the concentrator's aperture.

$$\eta_{oRec} = \frac{Q_u}{Q_{rec}} \quad (2)$$

In this case, Q_u, is the useful energy, in our case the energy that is delivered to the helical tube which contains the working fluid, and Q_{rec} is the amount of energy which is received by the receiver's aperture.

5- Cavity receivers design

The main part in the CSP is the receiver that functions as a connection link between the incoming energy (concentrated and reflected by the parabolic dish) and the working fluid, compressed air, inside the receiver. The latter is the one which is going to deliver the energy to the system that will convert into the needed form of heat or kinetic energy. So the need for having an efficient receiver is highly requested by researchers. One of the main factors regarding the receiver is its size; it should be as small as possible in order to reduce the heat losses [34]. The three investigated geometries were drawn using SOLIDWORKS® 2015 with the same value of each surface area as well as the aperture diameters. Fig. 3 shows the three geometries of cavity receiver and enlarged part of the helical tube used in the analysis. There are two types of concentration ratio [34]; one is known as a geometric concentration ratio which is simply defined as the collector aperture area divided by the receiver surface area and the optical concentration ratio which is the averaged flux received by the receiver over the average one incident on the area of the collector. In this work the geometric concentration ratio was chosen to be only 5X and the optical one ranged from (25X to 30X) depending on the receivers' surface properties. Table 1 shows the dimensions for each; the collector and the three studied geometries.

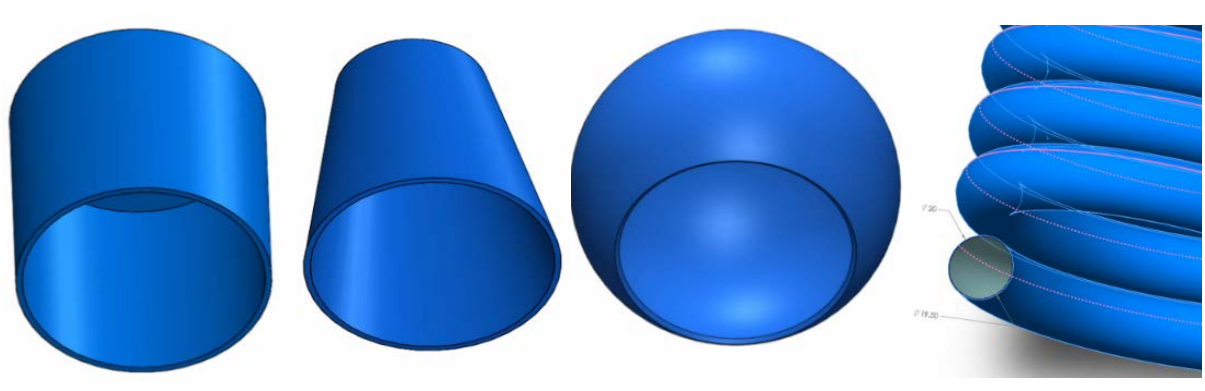

Fig. 3. The three designed geometry shapes of cavity receiver and the helical tube.

Table 1: Dimensions of the collector and the three receivers

Parameter	Collector	Cylindrical	Conical	Spherical	Tube
D (m)	1	0.20	*0.20*	*0.20*	*0.02*
t (m)	0.01	0.005	*0.005*	*0.005*	*0.00025*
Height (m)	-	0.2499	*0.3543*	*0.218*	-

6- Numerical simulation of the models

OptisWorks 2012 is simulation software used to simulate the optical performance of different concentrator solar collectors based on ray-tracing techniques. This tool has been intensively used by some researchers [40-47]. With the new features, especially the three-dimensional detector, the software is capable of seeing exactly what is going on inside the geometry of the cavity receiver and how the reflected flux is distributed on the cavity walls. In this work three different geometries of the thermal receiver, as shown in Fig. 3 (cylindrical, conical and spherical), are analyzed. The main aim of this simulation is to determine the effect of the shapes of the cavity configuration on the received and at the same time lost flux from the receiver. Consequentially, the modelled shapes have been simulated in OptisWorks® 2012, which is a three-dimensional ray-tracing technique, in order to determine the amount of received flux by the internal surface area of each receiver using a light source acting as the sun. The following summarized assumptions were considered for all cases, during the analysis: 1- The source was set to generate 10MW at radiation of 525 W/m^2 as a typical average radiation. 2- The source shape was defined as planar with a size larger than the aperture area of the parabolic collector in order to let the emitted incoming rays cover the aperture area of the three shapes. 3- Also, the ‘‘Lambertian” was used for intensity type and a limited half angle of 0^o was set. 4- The energy was simulated and equally divided to all the incident rays. 5- The concentrator was set to specular and has a reflectivity of 95%, highly polished material. The absorption ratio of the three receivers was set to 100%, 85% and 75% for this study.6- The detector that records the amount of incoming flux from the source as well as the reflected flux to the aperture area of the receiver is initiated and the helical tube inside each receiver takes the shape of the receiver configuration. 7- The material property of the receiver that was located at the focal point, which depends on the rim angle and diameter of the parabolic concentrator, was defined. Fig. 4 shows the flow diagram of simulation set-up in OptisWorks® software. Fig. 5 shows an example of concentrator parabolic reflector coupled with the thermal receiver and both of them are under the ray-tracing analysis.

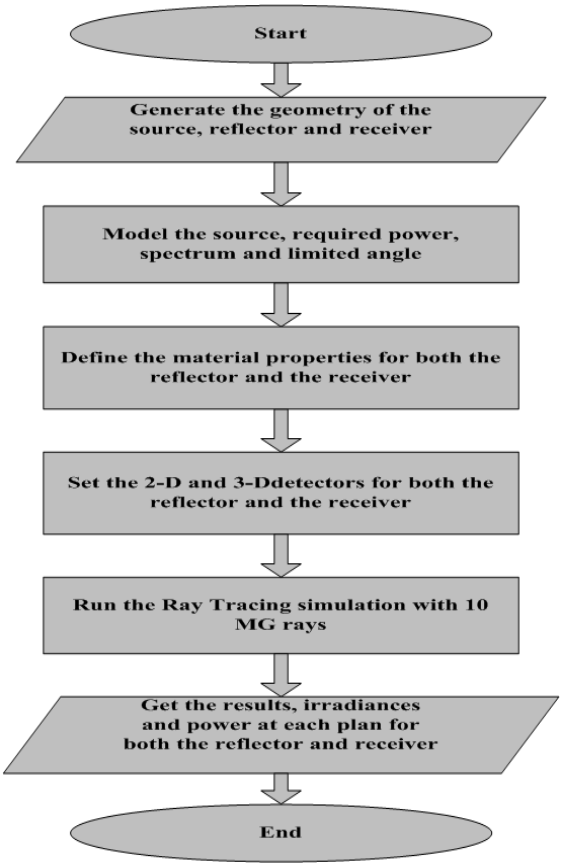

Fig. 4. Flow chart of modelling process of parapolic reflector and receiver using ray tracing technique.

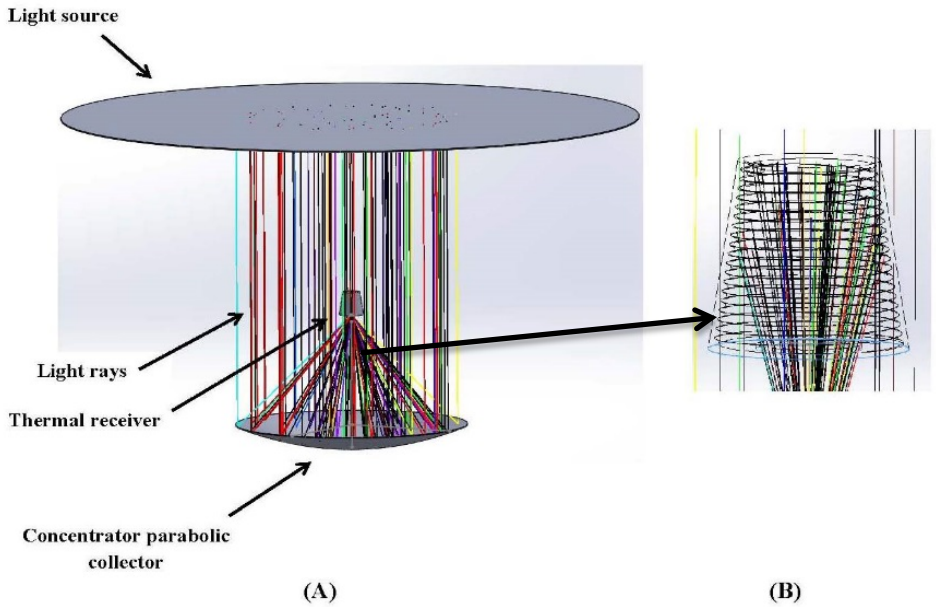

Fig. 5. OptisWorks® simulation (A): Parabolic concentrator with receiver. (B) Conical receiver.

7- Optical work validation

The simulated work carried out in this research has been validated against the experimental work found in [47], see Fig. 6. The two types of simulation (2-D and 3-D detectors) for this study have been investigated against the chosen experimental work. After designing similar geometry and set up the OptisWorks® software, the results of the both works were compared and good agreement was achieved. It can be noticed that the results of the 2-D detector is achieved with optical efficiency deviation about 7%, while 3-D detector results were closer to the experimental ones with a maximum deviation of about 4.5%. Thus the 2-D detector overestimates the results compared to the experimental value however the 3-D detector underestimate the results compared to the experimental work.

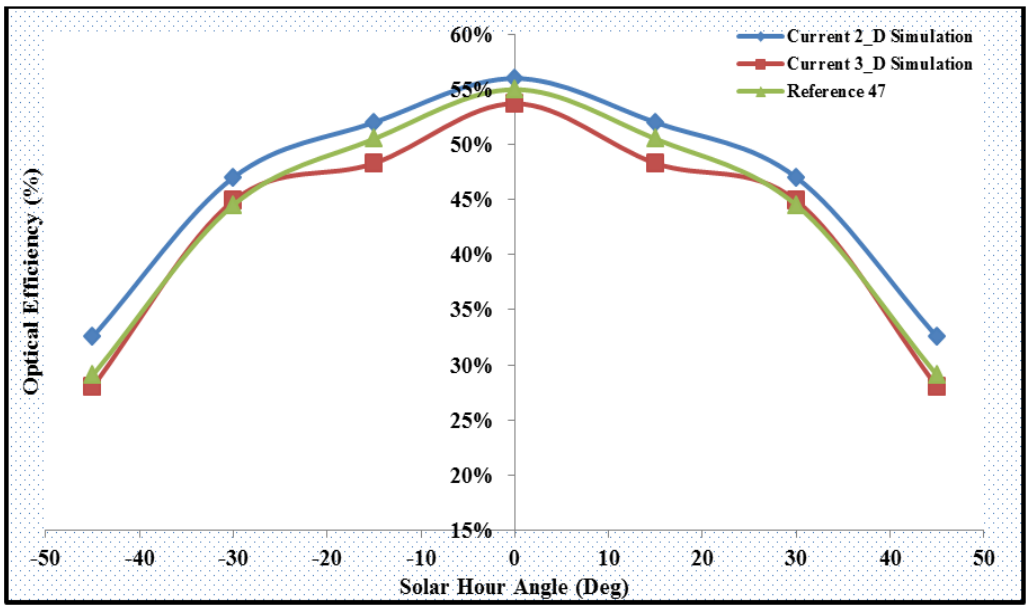

Fig. 6. Comparison the optical efficiency of the current study and reference [47].

8- Thermal analysis

For a comprehensive study and to cover the whole picture the thermal analysis was further investigated. Thus in the next section, the three configurations in terms of the amount of heat and losses have been evaluated. To be more precise, all the three modes of heat losses, conduction, convection and radiation were included in this analysis. The thermal analysis was based on the higher value of the absorption ratio of 85%, which was already investigated during the optical analysis.

8.1- Heat losses

The energy balance and the total heat losses can be determined using equations (3 and 4).

$$Q_T = Q_{Cond} + Q_{Conv} + Q_{Rad} \quad (3)$$

$$Q_T = mC_P(T_{fin} - T_{fout}) \quad (4)$$

While the three modes of heat losses: conduction, convection and radiation, are defined in equations (5-7) respectively [48 and 49].

$$\frac{\partial^2 T}{\partial X^2}+\frac{\partial^2 T}{\partial Y^2}+\frac{\partial^2 T}{\partial Z^2}+\frac{g}{k}=\frac{1}{\sigma}\frac{\partial T}{\partial t} \quad (5)$$

$$Q_{Conv}=hA \quad (6)$$

Where $h=kNu/L$

$$Q_{Rad}=\varepsilon\sigma(T_{Sur}^4-T_{Amp}^4) \quad (7)$$

Where $\varepsilon\ and\ \sigma$ are the emissivity and Boltzmann Constant respectively.

Calculating the heat transfer coefficient in terms of the Nusselt number required some factors to be considered. These factors are: the characteristic length of the model, the acceleration due to gravity, surface temperature, fluid temperature, dynamic viscosity, thermal conductivity and its specific heat.

In general, Nusselt numbers for laminar and turbulent free convection can be calculated using correlations (8 and 9) respectively [50 and 51].

$$Nu_{natu.\ Laminar}=0.508\left(\frac{Pr}{0.952+Pr}\right)^{1/4}Ra^{1/4} \quad (8)$$

$$Nu_{natu.\ Turbulant}=0.15\left(\frac{Pr^{9/16}}{0.671+Pr^{9/16}}\right)^{16/27}Ra^{1/3} \quad , where\ Pr=\frac{\upsilon}{\alpha} \quad (9)$$

Other correlations for Nusselt numbers' calculation, regarding cavity receivers' applications, have been proposed by many researchers, depending on their studied models and boundary conditions. The most well-known are those found in [19, 26, 52], which compute Nusselt numbers using equations (10-12).

$$Nu=0.54\ Ra^{1/4} \quad , where\ Ra=\frac{g\,\Delta T\,L_S}{\upsilon\alpha} \quad and \quad (10)$$

$$L_S=\left(4.79cos^{4.43}(\phi)-0.37\ sin^{0.719}(\phi)\right)D_{Cav}+\left(1.06cos^{3.24}(\phi)-0.0462\ sin^{0.286}(\phi)\right)D_{ap}+\left(7.07cos^{5.31}(\phi)-0.221\ sin^{2.43}(\phi)\right)L+$$

$$Nu_{D\,WI}=0.0303Gr_D^{0315}\left(1+cos(\phi)\right)^{3.551}\left(T_\omega/T_\infty\right)^{-0.086}\left(\frac{d_{ap}}{D_{Cav}}\right)^{0.878} for\ 10^6\le Gr\le 10^7 \quad (11)$$

$$Nu_D=0.0133Gr_D^{1/3}\left(1+cos(\phi)\right)^{2.6}\left(\frac{d_{ap}}{D_{Cav}}\right)^{0.47} \quad (12)$$

The radiative heat losses by contrast can be calculated based on radiosity, view factor and the emissivity of that configuration. The internal surface of the receiver is separated to a satisfied number of elements and each of those elements has either the same or different emissivity and temperature values; the radiosity at each element can be calculated using equation (13):

$\sigma T_{w,1}^4 = J_1 + \left(\frac{1-\varepsilon_I}{\varepsilon_I}\right)\sum_{j=1}^{N} F_{i,j}\left(J_i - J_j\right)$, where J and F are the radiosity and the view factor; i and j are any two surfaces inside the cavity. *(13)*

Then the total heat losses are determined using equations (14 and 15), [53-55].

$$Q_{Rad\,i} = \sum_{j=1}^{N} F_{i,j}\left(J_i - J_j\right) \quad (14)$$

$$Q_{Rad} = \varepsilon_{eff}\sigma\, A_{ap}\left(T_{wall}^4 - T_{amp}^4\right), where\ \varepsilon_{eff} = \frac{1}{\left(\frac{1-\varepsilon}{\varepsilon}\right)}\frac{A_{ap}}{A_w} \quad (15)$$

8.2- CFD Modelling and procedure

Once the three investigated geometries were drawn using SOLIDWORKS® 2015 with the same value of each surface area as well as the aperture diameters, then transferred to the ANSYS Fluent 15 Fig. 7, with the aim of determining the amount of heat losses and energy transferred by the HTF.

The continuity, energy and Navier-Stokes momentum equations (16- 18) simultaneously were employed to control the flow of the fluid in the curve tubes.

For this study single phase fluid is used under a steady state condition. The well-known k-ε viscous model was used for simulation due to its low computational cost with respect to the computation of the turbulent viscosity; moreover it is widely validated in engineering applications [56 and 57].

The 3-D tetrahedral element type of a smooth medium size was chosen [58]. In order to achieve the convenient mesh size configuration, a grid independence test was implemented for the chosen mesh, Fig. 8.

The assumptions during the analysis were summarized as follows: 1- The influence of gravitational force was included and the air was chosen as a HTF; the inlet temperature was fixed at 375 K due to the heat added from the compressor during compression. 2- The mass flow rate at the inlet was 0.01 Kg/s. This value is sufficient for the small scale turbine design which was included in the cycle mentioned in Fig. 1. 3- Highly insulated material has been assumed to be present on the outer receivers' cavity walls, see Table 2, in order to decrease the conduction heat losses. 4- The outlet condition was maintained at atmospheric pressure and the wind effect was neglected for the lower amount of convection heat loss. 5- Receiver geometry angle was fixed at 90^o to provide lower heat losses [25, 59-61]. 6- The surface to surface (S2S), radiation model was employed as a solution method for the calculation of the view factors, which are used for radiation heat losses' analysis [58].

Due to the small scale system and the lower amount of energy transferred, the convergence criteria for the residuals of both continuity and the velocity equations were decreased to the order of 10^{-5}; while the energy equation was decreased to 10^{-7} for the sake of precise comparison. The solutions were obtained once the convergence criteria were satisfied.

$$\frac{\partial \rho}{\partial t} + \frac{\partial}{\partial x_i}(\rho u_i) = 0 \quad (16)$$

$$\frac{\partial}{\partial t}(\rho u_i)+\frac{\partial}{\partial x_i}(\rho u_i u_j)=\frac{\partial}{\partial x_j}\left[-\rho\delta_{ij}+\mu\left(\frac{\partial u_i}{\partial x_j}+\frac{\partial u_i}{\partial x_i}\right)\right]+\rho g_i \quad (17)$$

$$\frac{\partial}{\partial t}(\rho C_P T)+\frac{\partial}{\partial x_i}(\rho u_i C_P T)-\frac{\partial}{\partial x_i}\left(\lambda\frac{\partial T}{\partial x_i}\right)=S_T \quad (18)$$

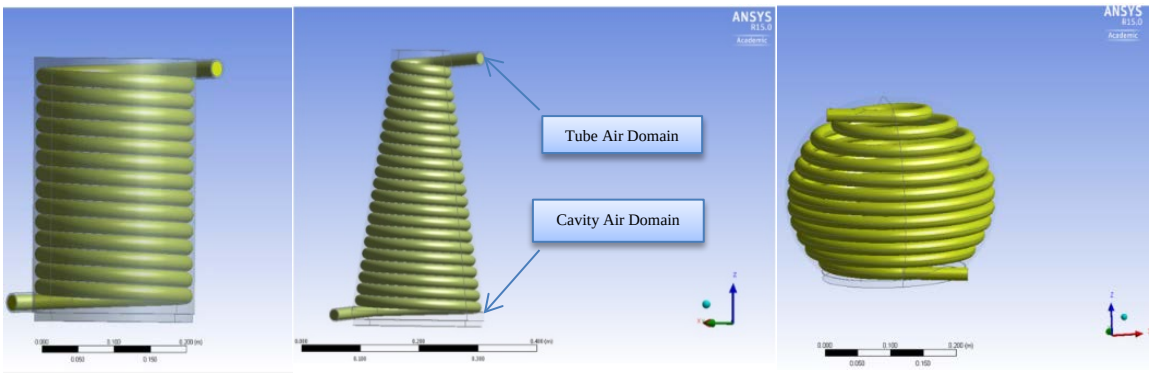

Fig.7. The three shapes of receiver modelled in ANSYS® modular.

Table 2: Material properties of the receiver

Properties	*Tube material (Copper)*	*Highly insulating material*
ρ (kg/m^3)	*8978*	*50*
Cp (J/kg.K)	*381*	*800*
k(W/m.K)	*387.6*	*0.09*

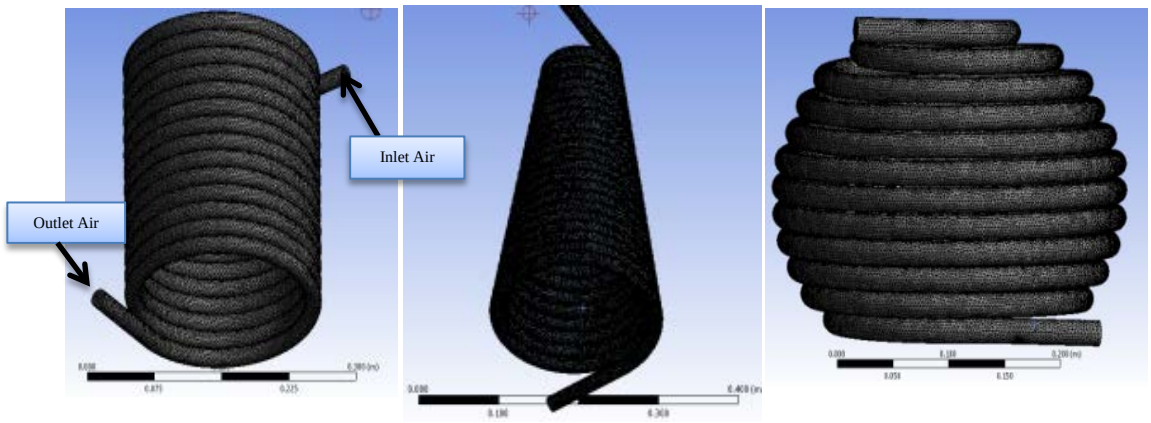

Fig. 8. 3-D Tetrahedral mesh for helical tube of the three receivers.

9- Thermal work validation

References [59, 60, 61 and 62] have been chosen as a validation source for the current study, due to their high reliability and the sufficient details of the data. The results demonstrated good agreement with the aforementioned references. The comparison between the present work and the four mentioned research studies found in literatures is shown in Fig. 9. The current work demonstrated that the data was compatible with the references, especially the model proposed by ref. [61], where the current work's result was closely matched. The current study revealed underestimated values for all the convective heat loss values through all the receiver inclinations in comparison with

the other references. This could be due to the assumed zero velocity value inside the cavity, which is considered different to the experimental cases.

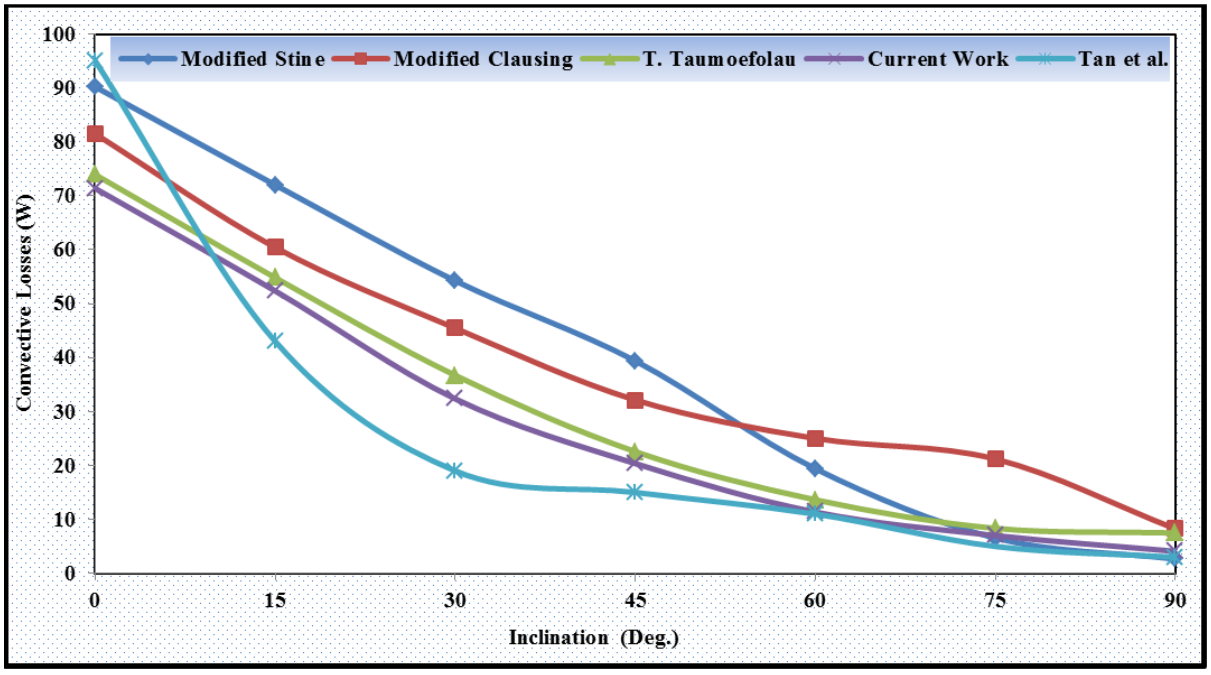

Fig. 9. Comparison the convective losses of the current study and other References.

10- Results and discussion

10.1- Effect of receiver walls' absorption ratio

The effect of the absorption ratio value for the internal wall surfaces of the cavity receivers is evaluated based on the received, reflected, absorbed rays. Also, the manner in which the flux is distributed inside the cavity receivers is discussed using the 3-D detector technique that is available in the new version of OptisWorks® 2012. This 3-D detector enables the researchers to observe how the flux is distributed inside each of the cavity receivers; as a result the dead areas and highly concentrated areas inside the cavity can be identified. These two important areas are undesirable in the design of cavity receivers, because they decrease the receiver's efficiencies (dead areas) and lead to more heat losses, as well as increasing the thermal stresses (highly concentrated areas). For example, the highly concentrated areas in the cavity receivers create hot spots which cause material threshold and this may lead to material failure in the receiver. The rays as well as the flux distribution for the three geometrical shapes, spherical, conical and cylindrical, at various absorption ratios of the internal surface are shown in Figs. 10a, 10b and 10c respectively. At this point it is important to emphasise that all of the three shapes were investigated at the same focal length and with the same positions of the cavity receivers. In terms of the amount of reflected rays, it is clear that this amount is directly proportional with the absorption ratio which is taken into consideration for the cavity shape of the receiver. However, it is not always the case that those reflected rays are considered as energy loss leaving the cavity shape; instead they are influenced by the geometry shape. For example, at absorption ratio of 85%, the ratio of the rays, which are reflected and lost out from cavity, is much higher in the spherical geometry comparing to the other two shapes (conical and cylindrical). While the minimum loss due to the reflection rays is occurred on the conical shape. Furthermore, the flux

distribution for each cavity shape was also directly affected by the geometry. For instance, there is a big difference in the amount of lost rays between the spherical and the cylindrical geometries. It can be seen that when the flux was uniformly distributed in the cylindrical shape, which has the best distribution among the others, some areas in spherical geometry were suffering from a lack of flux and at the same time some other areas were highly fluxed. At absorption ratio of 75%, the scenario is not much different from the one discussed previously except that the amount of lost reflected rays is higher. For the ideal case of 100% absorption ratio when it is assumed that all the rays which are hitting the cavity geometry are absorbed by its surface, it can be noticed that the geometry has almost no strong rule on the reflected rays. However, it does have an influence on the ratio of fluxed area inside each cavity which is depending on the position of the hitting rays which comes from the reflector. So in this case the worst flux distribution was for the spherical cavity where the difference between the highly fluxed areas and the ones with zero flux is very big.

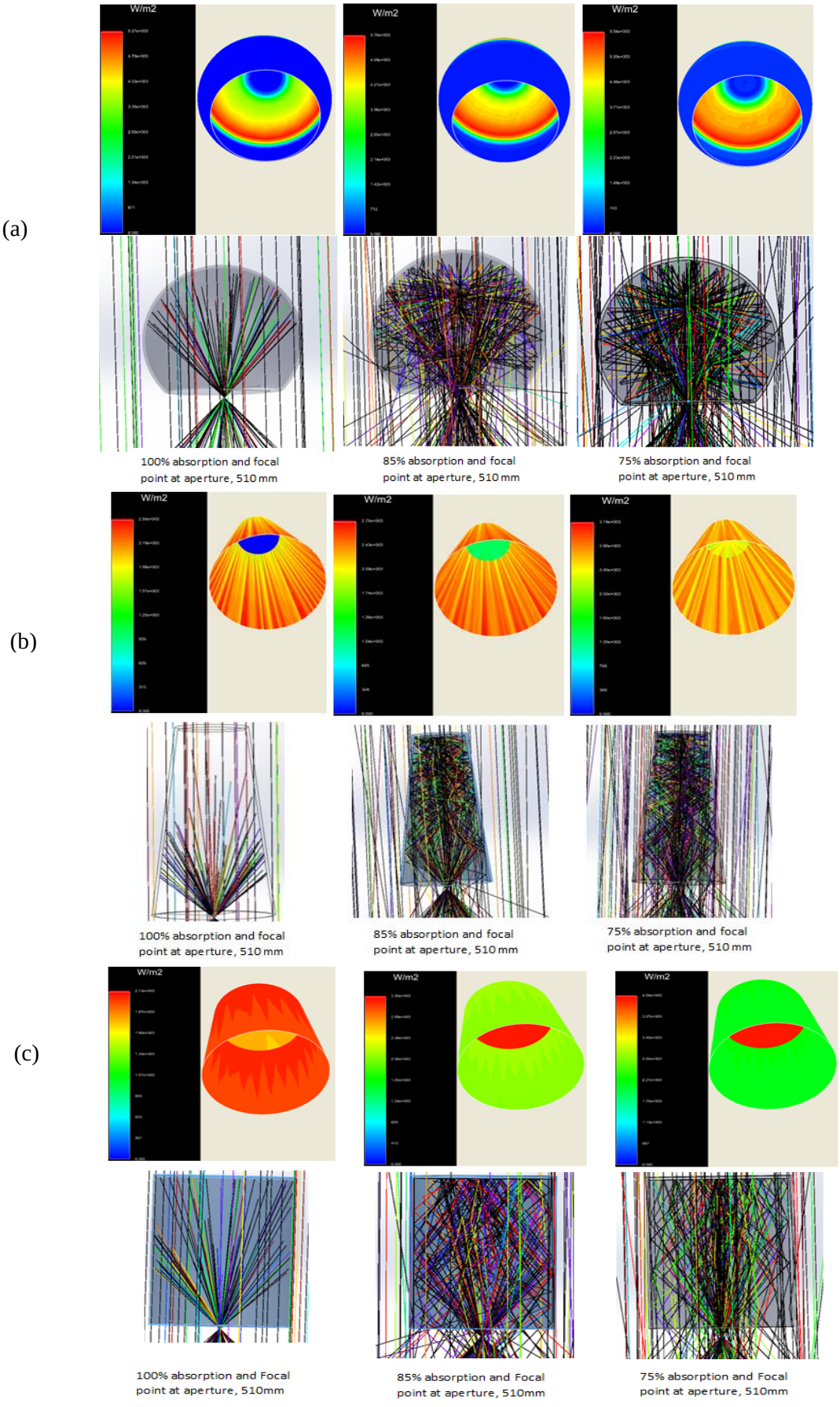

Fig. 10. The effect of absorption ratio on the rays and flux distribution of (a) Spherical shape, (b) Conical shape and (c) Cylindrical shape.

10.2- Effect of receiver's position

The influence of the receiver's position with respect to the focal point was thoroughly investigated. The cavity shape has also been considered in order to discover the behaviour of the rays, and flux distribution, with each cavity shape and position. The 3-D detectors again assisted the researchers with the visualisation of the behaviour of the rays and at the same time, with the analysis of their results. Figs. 11a, 11b and 11c show the results of this effect for the three studied positions for the spherical cavity shape at three different absorption ratios including: 100%, 85% and 75%, respectively. In Fig. 10a, where the assumed absorption ratio is 100%, the effect of changing the receiver position, with respect to the focal point can be seen. The worst distribution of flux happened when the focal point was located inside the spherical cavity; the best however, is when the geometry was shifted away to allow the focal point to be located outside the geometry. Similar behaviour can also be noticed when the absorption ratios were assumed to be 85% and 75%, Figs. 11b and 11c respectively. However, the amount of the received flux as well as the areas that most of the flux was concentrated (the tips) for the last two cases Figs. (11b and 11c) differ from the one showed in Fig. 11a. These areas are the tips of the spherical cavity receiver. Similarly, Figs. 12a, 12b and 12c show the effect of changing the conical shape position with respect to the focal point at three different absorption ratios; 100%, 85% and 75%, respectively. In Fig. 12a where the absorption ratio is 100%, the effect of varying the receiver position with respect to the focal point can be observed. The tip area was almost unaffected by changing the receiver position. However the amount of received flux was the highest compared to the other cases in Figs. (12b and 12c). Fig. 12b shows that the chance to get the best flux distribution is when the geometry was shifted toward the reflector's direction and the focal point located inside the geometry (at 85% absorption ratio). However, this was not the case when the absorption ratio was assumed to be 75% as shown in Fig. 12c which shows that better distribution was achieved by shifting away the receiver's position from the reflector's direction which allows the focal point to be located outside the geometry. In the same way Figs. 13a, 13b and 13c show the rays and the flux distribution for the cylindrical cavity receiver. In case of 100% absorption, it is clear that the best distribution happened when the focal point is at the aperture plane. However, this was not always the case when the assumed absorption ratios were considered to be 85% & 75% as shown in Figs. 13b & 13c respectively. As it can be seen in Figs. 13b & 13c the best distribution was observed to be when the geometry was shifted away, from the reflector's direction, to allow the focal point to be located outside the geometry.

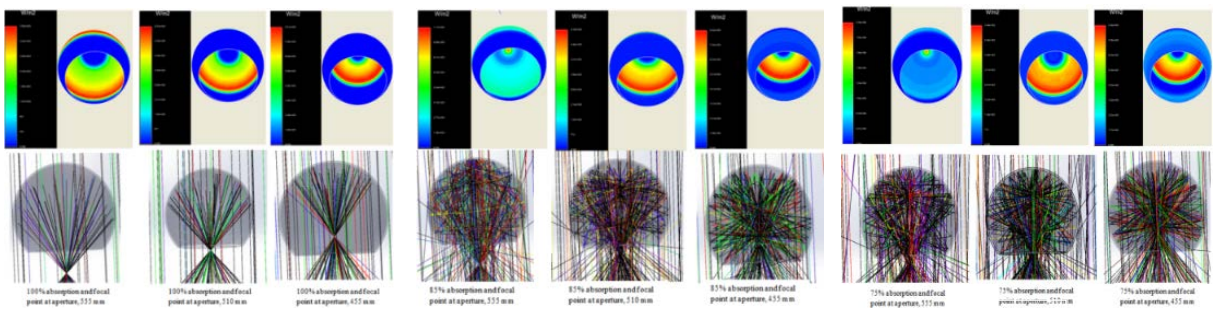

(a) (b) (c)

Fig. 11. The effect of receiver position on the rays and flux distributions for; (a) 100%, (b) 85% and (c) 75% absorption ratios.

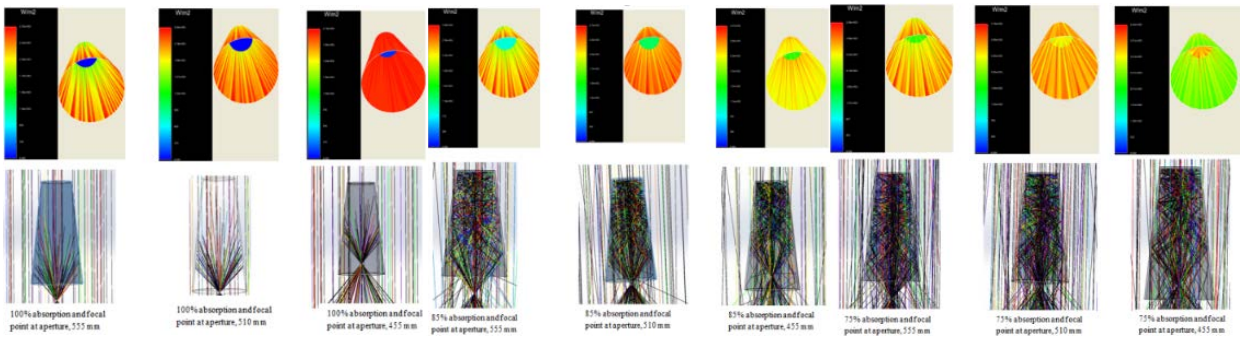

(a) (b) (c)

Fig. 12. The effect of receiver position on the rays and flux distributions for; (a) 100%, (b) 85% and (c) 75% absorption ratios.

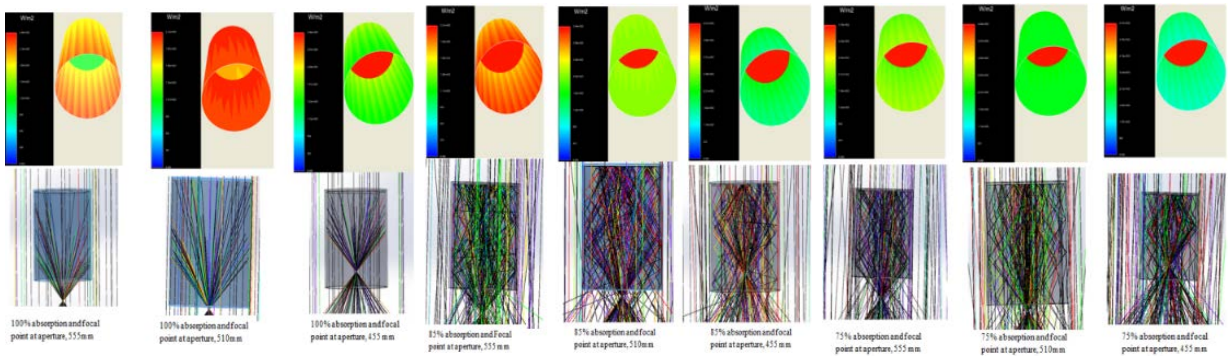

(a) (b) (c)

Fig. 13. The effect of receiver position on the rays and flux distributions for; (a) 100%, (b) 85% and (c) 75% absorption ratios.

In terms of numbers, the values of the total received and the absorbed energy by each cavity shape of the receivers are clearly affected by the absorption ratio, geometry and the position of the geometry with respect to the focal point. Figs. 14a- 14f show each total energy and absorbed energy amount for each cavity shape for the three types of receivers simulated in Figs. 11 to 13. From these Figures it is clear that the total energy that hits the cavity geometries is higher at lower absorption ratios. However, the absorbed energy by the cavity geometries' walls is directly proportional to the absorption ratio. It is noted that each of these energy values has its own value, which varies depending on each cavity shape as well as absorption ratio.

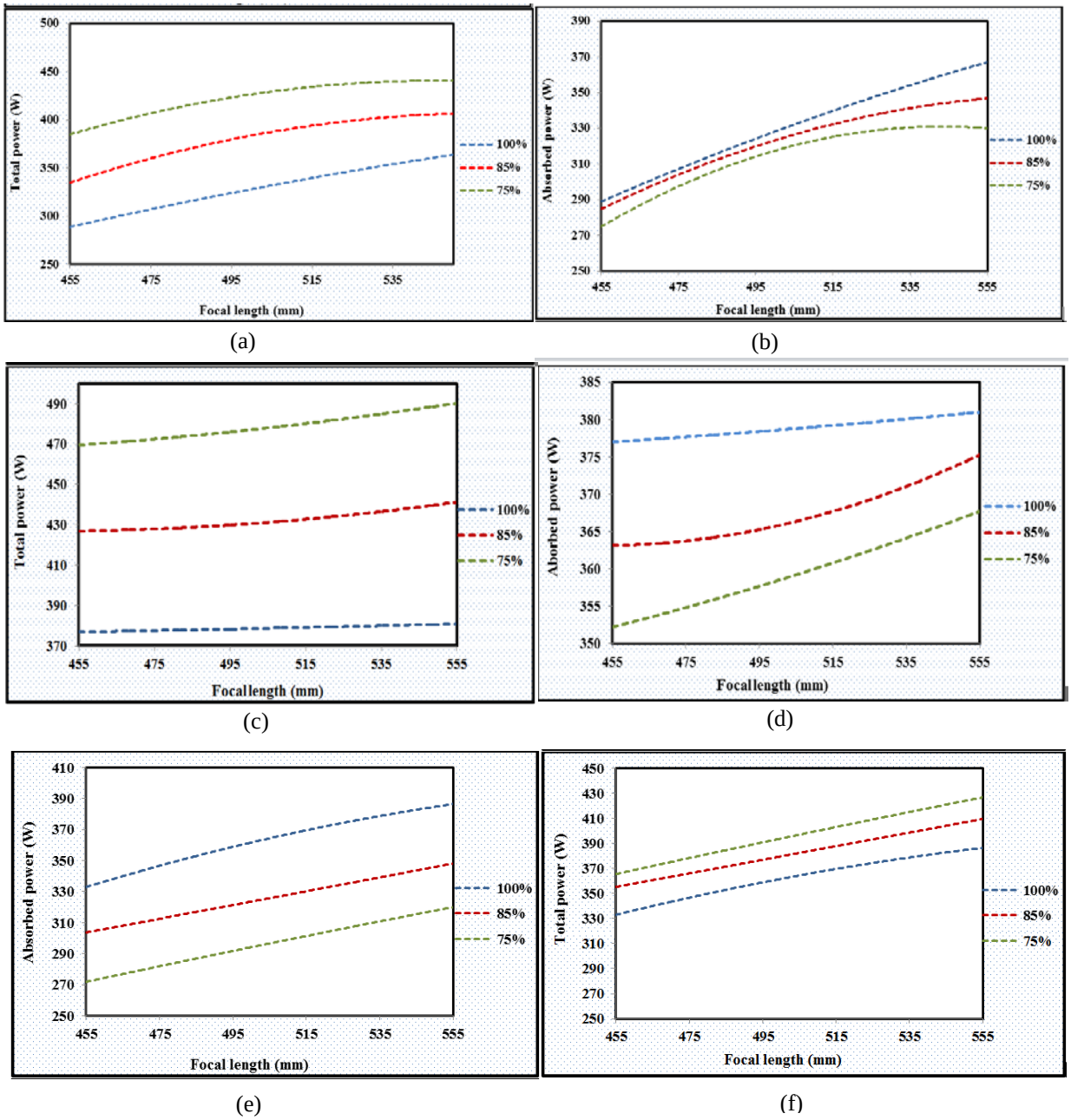

Fig. 14. Total and absorbed energy for the three mentioned positions falls on; the spherical shape (a & b), the conical shape (c & d) and the cylindrical shape (e & f).

Further investigation was carried out to identify the effect of the receivers at various positions, using the two assumed absorption ratios of 75% and 85%.

Figs. 15a- 15f show the trend that each shape has followed in terms of total and absorbed energy values. In Figs. 15a & 15b, the maximum energy values received and absorbed were located at 570 mm and 565 mm for 75% and 85% absorption ratios respectively. Similarly Figs. 15c & 15d show that the accompanying distances for maximum energy values received as well as absorbed were 560 mm and 555 mm. These two distances are for 75% and 85% absorption ratios respectively. For the cylindrical shape, Figs. 15e& 15f, the energy values reached the top at 585 mm and 590 mm when the assumed absorption ratios were 75% and 85% respectively. Furthermore three polynomial

correlations, with relatively high regression and R- squared values which are between about (0.918 and 0.962) were proposed. These relations, summarized in Table 3, can figure out the behaviour of the total energy values with respect to the position of the cavity receiver's shape.

Table 3: The three proposed correlations

Correlation	Shape	Total received energy (W)	R^2
$y = -0.0005x^3 + 0.8184x^2 - 441.77x + 79851$	Conical	at an of 75% absorption ratio	0.962
$y = -0.00005x^3 + 0.0599x^2 - 20.609x + 1964$	Conical	at an of 85% absorption ratio	0.9356
$y = -0.0003x^3 + 0.5053x^2 - 270.11x + 48417$	Spherical	at an of 85% absorption ratio	0.9187

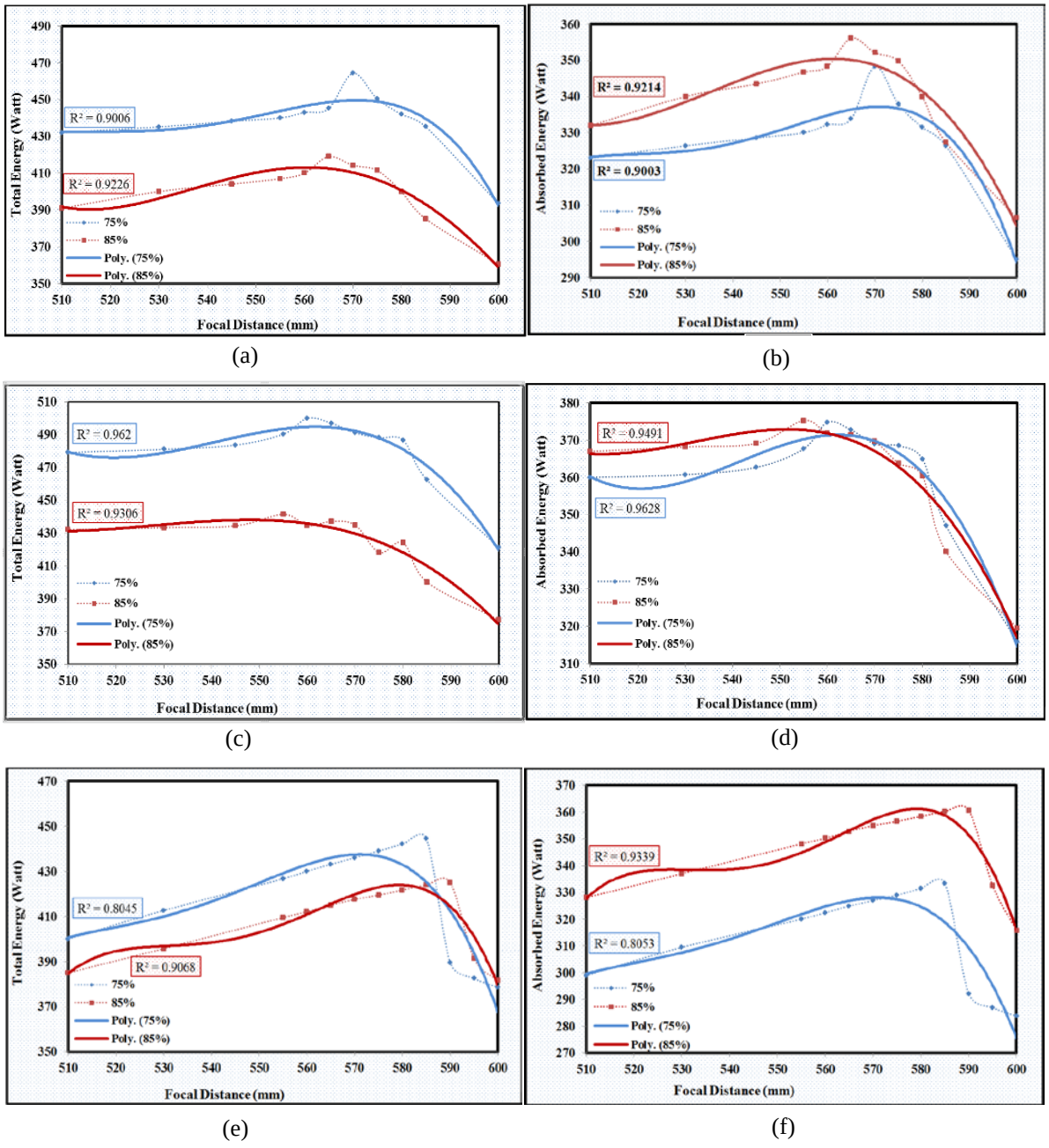

Fig. 15. Total and absorbed energy for at different receiver positions falls on; the spherical shape (a & b), the conical shape (c & d) and the cylindrical (e & f) shape.

10.3- Effect of receiver's cavity shape

It is clear that the geometry shape itself has a role in terms of the amount of energy received, absorbed, reflected and lost. After the rays hit the cavity wall they have two different probabilities, either to be directly absorbed by the wall or reflected by the internal cavity surfaces. The absorbed rays are considered as useful energy. However the reflected rays also have two different possibilities. They either hit another part of the cavity surface area and by doing so those rays will have the chance to be absorbed by the internal cavity walls and counted as useful energy, or they might go directly outside the cavity geometry through the aperture area and they will be considered as lost energy. Therefore the geometry shape of the receiver plays an important role in terms of reflected rays as well as the number of times that these rays are going to be reflected. As a result the effect of the receiver's geometry is examined in order to know which path each geometry has followed.

From Figs. 16a- 16d it is clear that the conical shape has received and absorbed the highest amount of energy compared to the other two receivers' configurations. However, the maximum energy values received and absorbed are different for each cavity shape at each proposed receiver absorption ratio. Specifically, at an absorption ratio of 75%, the maximum absorbed energy for the spherical, conical and cylindrical shapes was about 349, 375 and 333 watts at 570, 560 and 585 mm respectively. However, these values were about 355, 378 and 360 watts at 565, 555 and 590 mm respectively at an 85% absorption ratio.

The next part in this study contains a comparison between the three receiver geometries in terms of optical efficiency. Therefore, Figs. 17a & 17b show the optical efficiency of the three shapes at the range of receiver positions.

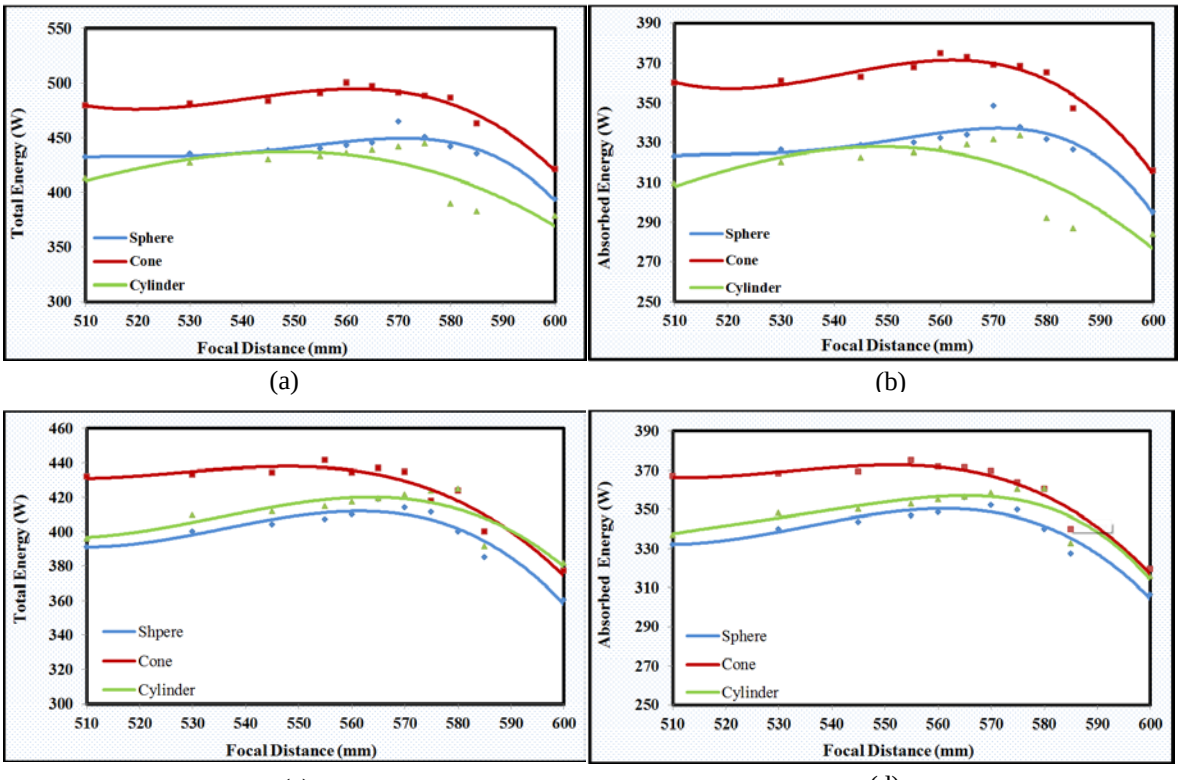

Fig. 16. Total and absorbed energy for the three cavity receivers at different receiver positions and absorption ratios of; 75% (a & b) and 85% (c & d).

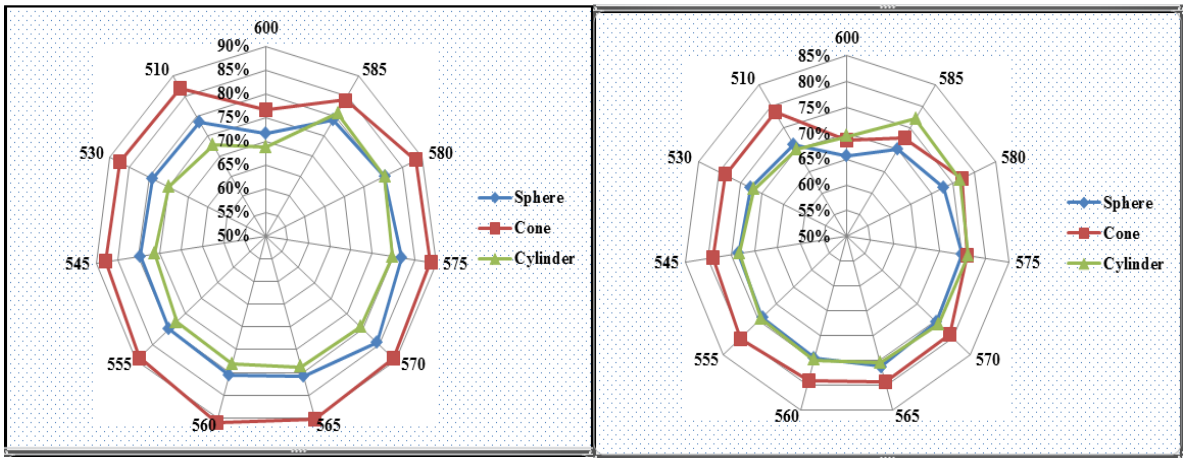

(a) (b)

Fig. 17. Optical efficiency for the three cavity receivers at different receiver positions (mm) and absorption ratios of; (a) 75% and (b) 85%.

Again, the superiority of the conical cavity receiver is clear among the other three shapes. It hits the tip with about 91 % and 82 % optical efficiency for 75% and 85% absorption ratios respectively. The cylindrical shape achieved the lowest optical efficiency at a 75% absorption ratio; however, at an 85% absorption ratio the optical efficiency values of both the cylindrical and spherical geometries were almost equal.

10.4- Thermal Results

The results are calculated based on the amount of heat absorbed by the helical tube inside the cavity of each of the three configurations, taking in consideration the amount of optical losses. The helical tube always takes the shape of the receiver cavity. The receiver shape has an important effect on the distribution of the received flux and consequently the amount of heat loss. Fig. 18 presents the effect of the amount of absorbed energy by the walls of the three configurations. Based on the optical behaviour of each shape, the amount of thermal flux that hits the walls of the three shapes will be different. Even though the best case optically (for each receiver shape) has been chosen to be thermally studied, some dead areas are noticed in the bottom of each of the three helical shapes.

Fig. 19 demonstrates the temperature distribution for the helical tube walls inside the three types of cavity receiver. The tube inlet air domain (from the compressor) starts at the top with a relatively low temperature; then the temperature is increased with each turn of the helical tube due to the radiated heat flux, until it reaches its final temperature at the end of the tube length.

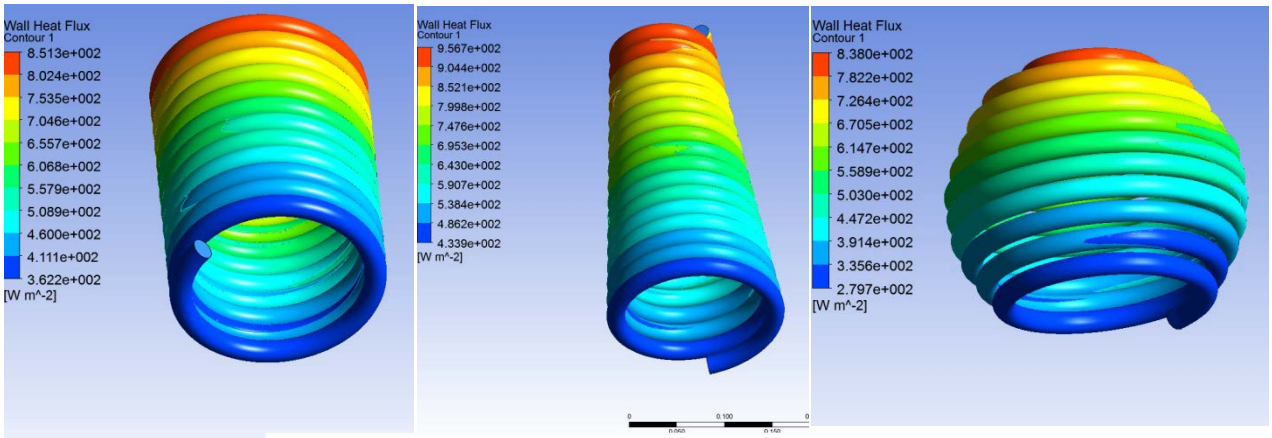

Fig. 18. The best (achieved) flux distribution for the three receivers.

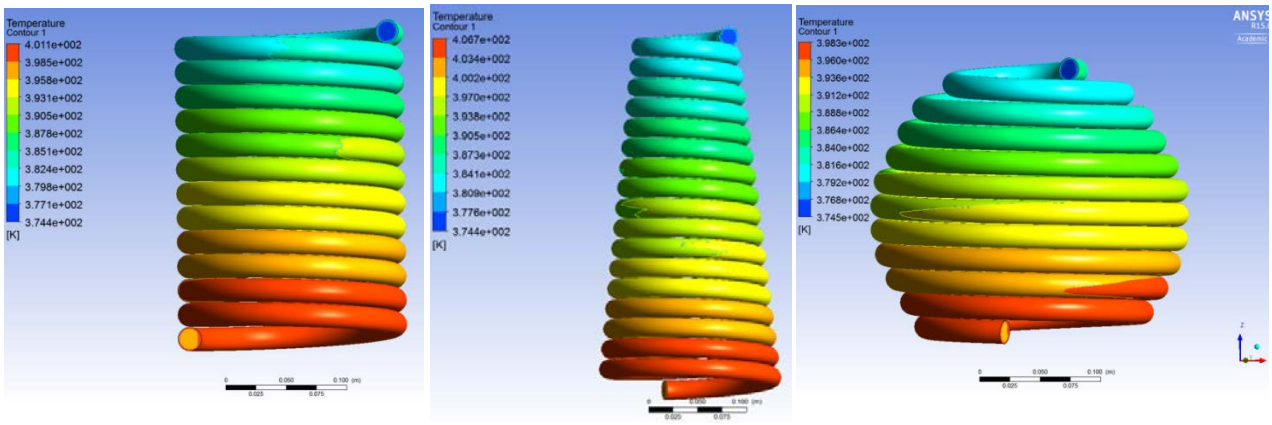

Fig. 19. Temperature distribution for the three receivers.

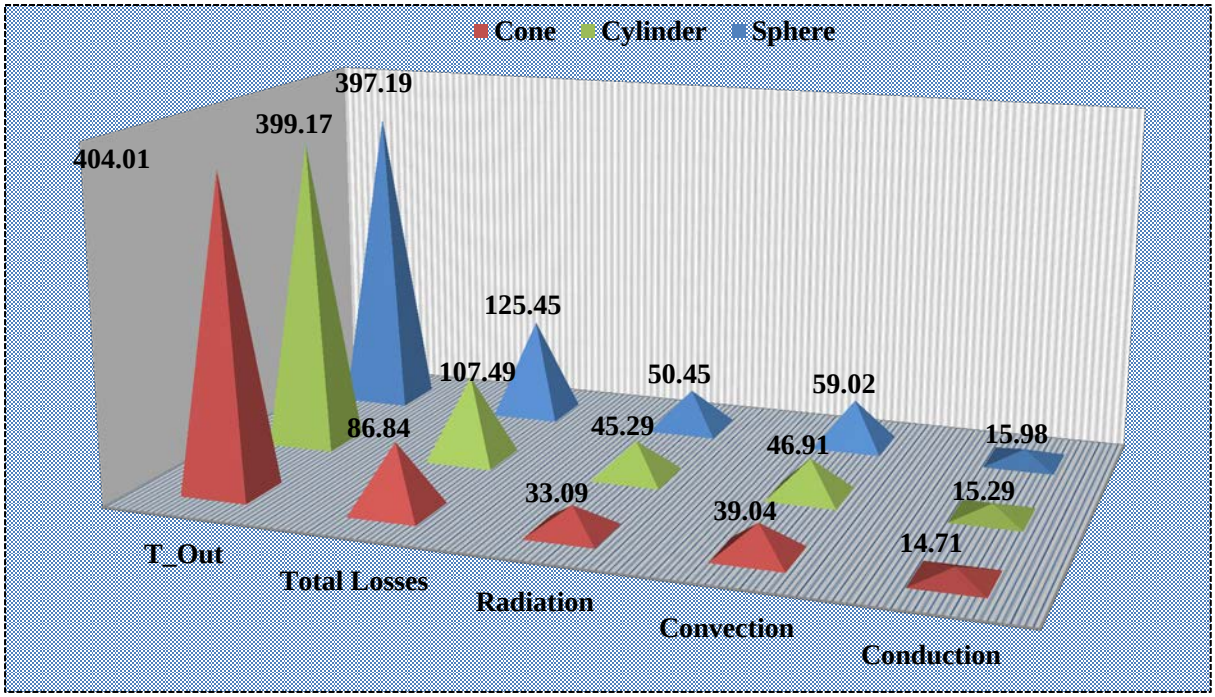

Fig. 20. Conductive, convective, radiative, total heat losses (watt) and outlet temperature of air (K) for the three shapes.

The conduction, convection, radiation, total amount of heat losses and the outlet temperature values for the three shapes are shown in Fig. 20. From this Figure it is noticed that the amount of convective heat losses were higher, due to the relatively low temperature of the three shapes. The conductive yielded the lowest losses; due to the highly insulating material covering the external surface of the three shapes during the numerical analysis.

Furthermore, the conical cavity shape experienced the lowest total heat losses and consequently produced the highest exit temperature, 404 K, compared to the other two geometries. The total heat losses' values were about 86, 107 and 125 watts for the conical, cylindrical and spherical cavity shapes respectively. The radiative heat losses of the conical, cylindrical and spherical cavity shapes were approximately 38.3%, 42.1% and 40.2 % of the total heat losses respectively; implying that the spherical shapes were the worst in terms of the amount of heat losses. The difference in the three

outlet temperature values was relatively small because of the small heat source (less than 400 watts) which was employed for this study. Finally, the overall optical and thermal efficiency of the three shapes was determined and displayed in Fig. 21.

The conical shape demonstrated the highest efficiency among the three shapes, as a result of being the best optically and thermally efficient in the analysis; approximately 8% higher compared to the cylindrical shape and ≈ 13% higher than that of the spherical shape.

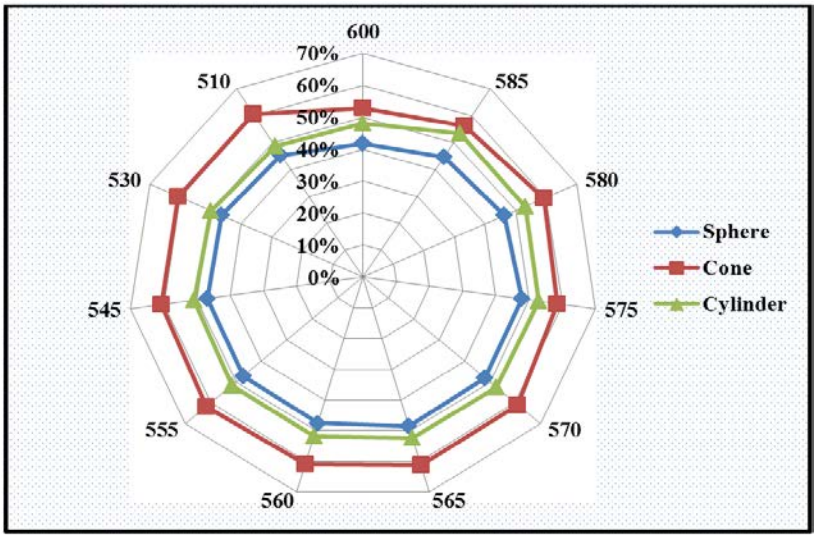

Fig. 21. Combined, optical and thermal efficiency, for the three cavity receivers at different receiver positions (mm) and absorption ratio of 85%.

11- Conclusions

Simulation work using cylindrical, conical and spherical shapes for a cavity receiver was developed with the objective of analysing their behaviour optically using the ray tracing method in OptisWorks® and thermally using ANSYS Fluent software. The results of the simulated work are validated using the experimental work found in the literature. The outcome of the current study has been concluded using the following points:

1- The conical shape receiver received and absorbed a higher amount of useful energy compared to the other two shapes; with about 6.5% and 12.5% at 85% and 75% absorption ratios respectively.
2- The focal point location changes with respect to the receiver shape, as well as the value of its absorption ratio. The maximum energy values were received and absorbed by the conical shape when it was located at 570 mm and 565 mm for 75% and 85% absorption ratios respectively; for the spherical shape at 560 mm and 555 mm for 75% and 85% absorption ratios respectively; and for the cylindrical shape at 585 mm and 590 mm for 75% and 85% absorption ratios respectively. From all the geometrical shapes developed and simulated in this research work the cylindrical shape has achieved the best flux distribution.
3- The R^2 values reached up to about 0.92, 0.98 and 0.93 for the spherical, conical and cylindrical shapes respectively. From the regression analysis it can be seen that the established third order polynomial correlations can predict the amount of energy at each

specific position of the cavity geometries and at each of the two investigated absorption ratios. These correlations could be a useful tool for quick choice in order to avoid any arbitrary assumption of a cavity receiver in optical efficiency.

4- The simulated work was validated against experimental work with a maximum deviation of 7% at 45^{o} and 4.5 % at 15^{o} for the 2-D and 3-D detectors respectively. The lower deviation of the simulation work compared to the experimental work shows that the simulation was accurate enough to justify the results.
5- Thermally, the conical shape provided the lowest heat losses and consequently achieved the highest thermal efficiency, about 77.05% compared to the 69% and 63% of the cylindrical and spherical receivers respectively; which indicates that this type is more suitable for the small-scale solar Brayton cycle.

ACKNOWLEDGMENT

The author thanks the Higher Committee of Developing Education in Iraq HCED for funding this project.

References

[1] Thakkar, Vanita, Ankush Doshi, and Akshaykumar Rana. "Performance Analysis Methodology for Parabolic Dish Solar Concentrators for Process Heating Using Thermic Fluid."
[2] K. Lovegrove, and W. Stein. Concentrating solar power technology, 2012.
[3] LD Jaffe. Dish concentrators for solar thermal energy. J Energy 7(4) (1981):304-312.
[4] W.G. Le Roux, Solar tracking for a parabolic dish used in a solar thermal Brayton cycle.
[5] Zheng, Zhang-Jing, Ming-Jia Li, and Ya-Ling He. "Thermal analysis of solar central receiver tube with porous inserts and non-uniform heat flux." Applied Energy (2015).
[6] Yang, Xiaoping, et al. "Numerical simulation study on the heat transfer characteristics of the tube receiver of the solar thermal power tower." Applied Energy 90.1 (2012): 142-147.
[7] Yang, Minlin, et al. "Heat transfer enhancement and performance of the molten salt receiver of a solar power tower." Applied Energy 87.9 (2010): 2808-2811.
[8] Yang, Xiaoping, et al. "Numerical simulation study on the heat transfer characteristics of the tube receiver of the solar thermal power tower." Applied Energy 90.1 (2012): 142-147.
[9] Bader, Roman, et al. "An air-based corrugated cavity-receiver for solar parabolic trough concentrators." Applied Energy 138 (2015): 337-345.
[10] Fuqiang, Wang, et al. "Parabolic trough receiver with corrugated tube for improving heat transfer and thermal deformation characteristics." Applied Energy 164 (2016): 411-424.
[11] Padilla, Ricardo Vasquez, et al. "Heat transfer analysis of parabolic trough solar receiver." Applied Energy 88.12 (2011): 5097-5110.
[12] Mwesigye, A., Huan, Z., & Meyer, J. P. (2015). Thermodynamic optimisation of the performance of a parabolic trough receiver using synthetic oil–Al 2 O 3 nanofluid. Applied Energy, 156, 398-412.
[13] Wu, Zhiyong, et al. "Three-dimensional numerical study of heat transfer characteristics of parabolic trough receiver." Applied Energy 113 (2014): 902-911.
[14] Wu, Zhiyong, et al. "Experimental and numerical studies of the pressure drop in ceramic foams for volumetric solar receiver applications." Applied Energy87.2 (2010): 504-513.
[15] Roldán, M. I., and R. Monterreal. "Heat flux and temperature prediction on a volumetric receiver installed in a solar furnace." Applied Energy 120 (2014): 65-74.
[16] Mojiri, Ahmad, et al. "A spectral-splitting PV–thermal volumetric solar receiver." Applied Energy 169 (2016): 63-71.

[17] Anwar, M. Khalil, B. S. Yilbas, and S. Z. Shuja. "A thermal battery mimicking a concentrated volumetric solar receiver." Applied Energy 175 (2016): 16-30.
[18] Harris, James A., and Terry G. Lenz. "Thermal performance of solar concentrator/cavity receiver systems." Solar energy 34.2 (1985): 135-142.
[19] Wu, Shuang-Ying, et al. "Experimental study on combined convective heat loss of a fully open cylindrical cavity under wind conditions." International Journal of Heat and Mass Transfer 83 (2015): 509-521.
[20] Uhlig, R., et al. "Strategies enhancing efficiency of cavity receivers." Energy Procedia 49 (2014): 538-550.
[21] Reddy, K. S., T. Srihari Vikram, and G. Veershetty. "Combined heat loss analysis of solar parabolic dish–modified cavity receiver for superheated steam generation." Solar Energy 121 (2015): 78-93.
[22] W.G. Le Roux, T. Bello-Ochende, and J.P. Meyer. Operating conditions for an open direct solar thermal Brayton cycle with optimised cavity receiver and recuperator. Energy: doi:10.1016/energy. 2011.08.012
[23] Prakash, M. "Numerical Study of Natural Convection Heat Loss from Cylindrical Solar Cavity Receivers." ISRN Renewable Energy 2014 (2014).
[24] Kumar, N. Sendhil, and K. S. Reddy. "Numerical investigation of natural convection heat loss in modified cavity receiver for fuzzy focal solar dish concentrator." Solar Energy 81.7 (2007): 846-855.
[25] T. Taumoefolau and K. Lovegrove. An experimental study of natural convection heat loss from a solar concentrator cavity receiver at varying orientation. Australia, 2002.
[26] B. Abdullahia, R. K. Al-dadaha, S. Mouhmud. Optical Performance of Double Receiver Compound Parabolic Concentrator Energy Procedia 61 (2014) 2625 – 2628.
[27] Le Roux, Willem Gabriel, Tunde Bello-Ochende, and Josua P. Meyer. "The efficiency of an open-cavity tubular solar receiver for a small-scale solar thermal Brayton cycle." Energy Conversion and Management 84 (2014): 457-470.
[28] Qiu, Kunzan, et al. "Simulation and experimental study of an air tube-cavity solar receiver." Energy Conversion and Management 103 (2015): 847-858.
[29] Fleming, Austin, et al. "A general method to analyze the thermal performance of multi-cavity concentrating solar power receivers." Solar Energy (2015).
[30] A. Algaruea, S. Mahmouda, R.K. AL-Dadah, Optical Performance of Low Concentration Ratio Reflective and Refractive Concentrators for Photovoltaic Applications. Energy Procedia 61 (2014) 2375 – 2378.
[31] Wang, F., Lin, R., Liu, B., Tan, H., & Shuai, Y. (2013). Optical efficiency analysis of cylindrical cavity receiver with bottom surface convex. Solar Energy, 90, 195-204.
[32] Weinstein, Lee, et al. "Optical cavity for improved performance of solar receivers in solar-thermal systems." Solar Energy 108 (2014): 69-79.
[33] Tzivanidis, C., et al. "Thermal and optical efficiency investigation of a parabolic trough collector." Case Studies in Thermal Engineering 6 (2015): 226-237.
[34] Stine, William B., and Michael Geyer. "Power from the Sun." (2001).
[35] Mancini, Thomas, et al. "Dish-Stirling systems: An overview of development and status." Journal of Solar Energy Engineering 125.2 (2003): 135-151.
[36] Kribus, Abraham, et al. "A miniature concentrating photovoltaic and thermal system." Energy Conversion and Management 47.20 (2006): 3582-3590.
[37] Feuermann, Daniel, and Jeffrey M. Gordon. "High-concentration photovoltaic designs based on miniature parabolic dishes." Solar Energy 70.5 (2001): 423-430.
[38] Alaphilippe, Muriel, Sébastien Bonnet, and Pascal Stouffs. "Low power thermodynamic solar energy conversion: coupling of a parabolic trough concentrator and an Ericsson engine." International Journal of Thermodynamics 10.1 (2007): 37-45.
[39] Segal, Akiba, and Michael Epstein. "Optimized working temperatures of a solar central receiver." Solar Energy 75.6 (2003): 503-510.
[40] Ali, Imhamed M. Saleh, et al. "Optical performance evaluation of a 2-D and 3-D novel hyperboloid solar concentrator." World Renewable Energy Congress XI. 2010.

[41] Arnaoutakis, Georgios E., et al. "Enhanced energy conversion of up-conversion solar cells by the integration of compound parabolic concentrating optics." Solar Energy Materials and Solar Cells 140 (2015): 217-223.
[42] Sellami, Nazmi, and Tapas K. Mallick. "Optical efficiency study of PV crossed compound parabolic concentrator." Applied Energy 102 (2013): 868-876.
[43] Baig, Hasan, et al. "Performance analysis of a dielectric based 3D building integrated concentrating photovoltaic system." Solar Energy 103 (2014): 525-540.
[44] Arnaoutakis, Georgios E., et al. "Coupling of sunlight into optical fibres and spectral dependence for solar energy applications." Solar energy 93 (2013): 235-243.
[45] Sellami, Nazmi, and Tapas K. Mallick. "Optical characterisation and optimisation of a static Window Integrated Concentrating Photovoltaic system." Solar Energy 91 (2013): 273-282.
[46] Ali, Imhamed M. Saleh, et al. "An optical analysis of a static 3-D solar concentrator." Solar Energy 88 (2013): 57-70.
[47] Abdullahi, B., et al. "Optical and thermal performance of double receiver compound parabolic concentrator." Applied Energy 159 (2015): 1-10.
[48] Bergman, Theodore L., Frank P. Incropera, and Adrienne S. Lavine. Fundamentals of heat and mass transfer. John Wiley & Sons, 2011.
[49] A. Bejan, Heat Transfer, John Wiley & Sons, 1993.
[50] Eckert, E.R.G. (1950), Introduction to the Transfer of Heat and Mass, McGraw-Hill Companies, New York, USA, pp. 158-164.
[51] Churchill, S.W. and Chu H.H.S. (1975), Correlating Equations for Laminar and Turbulent Free Convection from a Vertical Plate, Int. J. Heat Mass Transfer 18, 1323-1329.
[52] Paitoonsurikarn, S., and K. Lovegrove. "On the study of convection loss from open cavity receivers in solar paraboloidal dish applications" Proceedings of Solar. 2003.
[53] Holman J.P. (1997) Heat transfer, 8th edition, New York: McGraw-Hill Companies.
[54] Jilte, R. D., S. B. Kedare, and J. K. Nayak. "Natural convection and radiation heat loss from open cavities of different shapes and sizes used with dish concentrator." Mechanical Engineering Research 3.1 (2013): 25.
[55] Wu, Y. C., and L. C. Wen. "Solar receiver performance of point focusing collector system." American Society of Mechanical Engineers 1 (1978).
[56] Duran, J. Esteban, Fariborz Taghipour, and Madjid Mohseni. "CFD modeling of mass transfer in annular reactors." International Journal of Heat and Mass Transfer 52.23 (2009): 5390-5401.
[57] Roldán, M. I., L. Valenzuela, and E. Zarza. "Thermal analysis of solar receiver pipes with superheated steam." Applied Energy 103 (2013): 73-84.
[58] Ansys fluent theory guide." http://www.ansys.com, 2015.
[59] Clausing, A. M. "An analysis of convective losses from cavity solar central receivers." Solar Energy 27.4 (1981): 295-300.
[60] Stine, William B., and C. G. McDonald. "Cavity receiver convective heat loss." International Solar Energy Society, Solar World Congress (1989, Kobe, Japon). 1989.
[61] Taumoefolau, T., et al. "Experimental investigation of natural convection heat loss from a model solar concentrator cavity receiver." Journal of Solar Energy Engineering 126.2 (2004): 801-807.
[62] Tan, Yuting, et al. "Experimental investigation on heat loss of semi-spherical cavity receiver." Energy Conversion and Management 87 (2014): 576-583.

Nomenclature

A: Area (m^2)
Aa: Aperture area (m^2)
Cp: Specific heat (J/kg.K)
d: Diameter (m)
ε: surface emissivity
f: Focal
F: View factor
g: Gravity (Kg)
Gr: Grashof Number
h: Height of receiver (m), Heat Transfer Coefficient
J: Radiosity
k: Thermal conductivity (W/m.K)
L: Characteristic Length (m)
m: Mass Flow Rate of Fluid
Nu: Nusselt Number
Pr: Prandtl Number
ρ: Density (Kg/m^3)
Q: Heat
Ra: Rayleigh Number
u: velocity component in x- direction (m/s)
T: Temperature (K)
t: Time (Sec)
μ: viscosity (kg/m.s)
η_o: Optical efficiency
ϕ : Receiver Inclination angle (Deg.)
x: Coordinate
ST: Energy source

Subscripts

1: Compressor Inlet
2: Recuperator Inlet of high pressure air
3: Receiver Inlet
4: Turbine Inlet
5: Recuperator Inlet of low pressure air
6: Recuperator Exit
Amb: Ambient
Ap: Aperture
Cav: Cavity
Cond: Conduction
Conv: Convection
i: coordinate
f: Fluid
natu: Natural
Rad: Radiation
Ref: Reflector
Rec: Receiver
Sur: Surface area
T: Total
W: Wall or cavity internal surface
WI: With insulation